Curvature-Induced Instabilities of Shells

Matteo Pezzulla,[1] Norbert Stoop,[2] Mark P. Steranka,[1] Abdikhalaq J. Bade,[1] and Douglas P. Holmes[1,*]

[1]*Department of Mechanical Engineering, Boston University, Boston, Massachusetts 02215, USA*
[2]*Department of Mathematics, Massachusetts Institute of Technology, Cambridge, Massachusetts 02139, USA*

Induced by proteins within the cell membrane or by differential growth, heating, or swelling, spontaneous curvatures can drastically affect the morphology of thin bodies and induce mechanical instabilities. Yet, the interaction of spontaneous curvature and geometric frustration in curved shells remains poorly understood. Via a combination of precision experiments on elastomeric spherical shells, simulations, and theory, we show how a spontaneous curvature induces a rotational symmetry-breaking buckling as well as a snapping instability reminiscent of the Venus fly trap closure mechanism. The instabilities, and their dependence on geometry, are rationalized by reducing the spontaneous curvature to an effective mechanical load. This formulation reveals a combined pressurelike term in the bulk and a torquelike term in the boundary, allowing scaling predictions for the instabilities that are in excellent agreement with experiments and simulations. Moreover, the effective pressure analogy suggests a curvature-induced subcritical buckling in closed shells. We determine the critical buckling curvature via a linear stability analysis that accounts for the combination of residual membrane and bending stresses. The prominent role of geometry in our findings suggests the applicability of the results over a wide range of scales.

Owing to their slender geometry, thin elastic shells display intriguing mechanical instabilities. Perhaps the most iconic example is the buckling of a spherical shell under pressure—a catastrophic situation that often leads to structural failure [1,2]. Instabilities and shape changes are also fundamental during the development and morphogenesis of thin tissue [3,4]. To control and evolve shape, nature heavily relies on internal stimuli such as growth, swelling, or active stresses [5,6]. If the stimulus varies through the thickness of the shell, it generally induces a change of the spontaneous (or natural) curvature of the tissue [7]. Examples are the ventral furrow formation in Drosophila [8] or the fast closure mechanism invoked by the Venus fly trap to catch prey [9]. Harnessing similar concepts for technological applications, internal stimuli were also suggested as a means to design adaptive metamaterials [10] and soft robotics actuators [11]. To describe the mechanics of slender structures with arbitrary stimuli, classical shell mechanics was extended recently to model bodies that do not possess a stress-free configuration [12–14], leading to the non-Euclidean shell theory [15]. Despite recent progress [16,17], the role of curvature-altering stimuli, and their interplay with geometric frustration and instabilities in thin, initially curved shells, remains poorly understood.

In this Letter, we combine precision experiments with non-Euclidean shell theory to reveal how curvature stimuli induce mechanical instabilities in spherical shells. Our experiments demonstrate symmetry-breaking as well as snap-through shape transitions depending on the amount of stimulus and the deepness of the shell. To rationalize our findings, we show that a curvature stimulus reduces to a pressurelike normal force in the bulk, but induces a torque along the boundary of the shell. A scaling analysis of the dominant boundary term allows us to construct an analytical phase diagram that captures well the transitions found in experiments and simulations. For closed spherical shells, we show that the pressurelike stimulus induces a curvature-controlled buckling instability. The critical stimulus is obtained from stability analysis and found to be in the range of related biological systems.

In our experiments, we uniformly coated a rigid sphere (radii $R \in [12, 75]$ mm) with silicone-based vinyl-polysiloxane (VPS) 32 (Zhermack), such that it thermally cross-links into an elastomeric shell [18]. We then repeated the coating process with VPS 8, and cut shells with opening angles $\theta \in [20, 150]°$, resulting in bilayer shells of thicknesses $h \in [0.5, 1.3]$ mm. Because of differential swelling between the two polymer layers, internal stresses develop. We quantify this geometric frustration by cutting a long, narrow strip from the shell. Free of any constraints, the strip adopts a shape with curvature $\bar{\kappa}$, which can be additively decomposed into the initial curvature $-1/R$ and natural curvature κ. Thus, $\kappa = \bar{\kappa} + 1/R$ measures the curvature stimulus [Fig. 1(a)] [17,19]. Specifically, for a bilayer with VPS 8 on the outside, we find $\kappa > 0$, and by switching the order of the layers, we can induce a negative natural curvature ($\kappa < 0$). To characterize the various geometries, we introduce the dimensionless parameter $\bar{\theta} = \theta/\sqrt{h/R}$, describing the deepness of the shell with respect to the angular width of the boundary layer $\sqrt{h/R}$ [20].
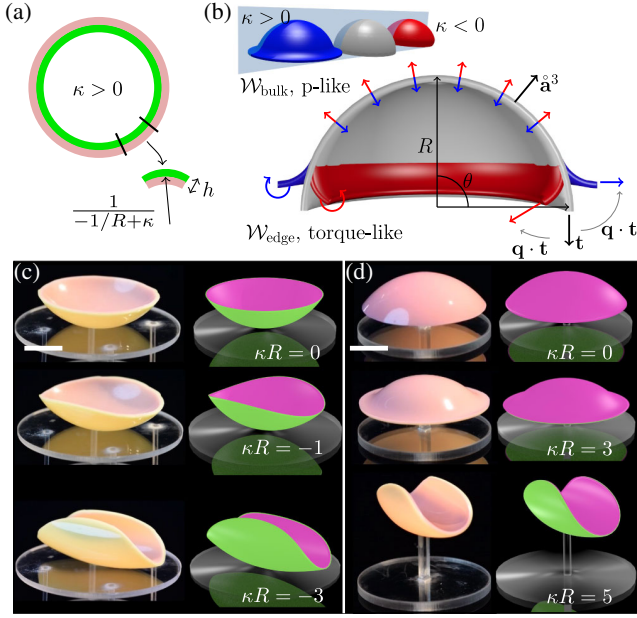
FIG. 1. (a) Schematic of a VPS bilayer shell with natural radius of curvature $1/(-1/R + \kappa)$ induced by residual swelling. (b) The natural curvature mechanically corresponds to torques on the boundary and a pressure field in the bulk. (c) Buckling of open spherical shells triggered by $\kappa < 0$ (left, experiments; right, simulations). (d) Snapping of open spherical shells triggered by $\kappa > 0$ for $\bar{\theta} = 5$. Scale bars 2 cm.

For shells with $\kappa < 0$, we find that the stimulus leads to a loss of rotational symmetry via a supercritical buckling bifurcation [Fig. 1(c)] [3]. Experiments suggest no strong dependence of this transition on $\bar{\theta}$. For $\kappa > 0$, the stimulus acts to evert the initial curvature of the shell. Above a critical stimulus, we observe a snap-through instability [Fig. 1(d)], reminiscent of the abrupt concave-convex shape changes employed by the Venus fly trap [9], and the embryonic inversion of *Volvox* [21]. Here, the critical curvature stimulus increases with $\bar{\theta}$. Moreover, shallow shells with $\bar{\theta} < \bar{\theta}_s \approx 2$ do not snap, whereas shells with $\bar{\theta} < \bar{\theta}_c \approx 4$ remain rotationally symmetric after snapping, while deep ones break the rotational symmetry during snap through (Fig. 2).

To explain the richness of the experimental findings, we rely on non-Euclidean shell theory, which has recently been proposed as a model for growth in thin, bidimensional bodies [15]. In this formulation, the mechanics of the shell is entirely described by the geometry of the middle surface with first and second fundamental forms **a**, **b** [22]. The undeformed reference configuration in absence of curvature stimulus is characterized by $\mathring{\mathbf{a}}$, $\mathring{\mathbf{b}}$, respectively. Curvature stimuli are modeled by changing the reference configuration to effectively generate stresses and moments arising from differential swelling of the shell layers [23]. The resulting natural configuration has fundamental forms $\bar{\mathbf{a}}$, $\bar{\mathbf{b}}$ and is generally not embeddable in Euclidean space.

When the stimulus does not induce a stretch of the midsurface ($\bar{\mathbf{a}} = \mathring{\mathbf{a}}$), one obtains $\bar{\mathbf{b}} = \mathring{\mathbf{b}} + \kappa\mathring{\mathbf{a}}$, where κ is the scalar (additive) natural curvature [23]. The energy of the shell may be written after some algebra as [24]

$$\bar{\mathcal{U}} = \bar{\mathcal{U}}_s^K + \frac{h^2}{3}\bar{\mathcal{U}}_b^K - \frac{2(1+\nu)h^2}{3}\int \kappa \operatorname{tr}(\mathbf{b} - \mathring{\mathbf{b}})d\omega. \quad (1)$$

Here, $\bar{\mathcal{U}}^K = \bar{\mathcal{U}}_s^K + h^2\bar{\mathcal{U}}_b^K/3$ is Koiter's classical shell energy composed of stretching and bending terms without any inelastic stimuli [24,29], ν is the Poisson ratio ($\nu = 1/2$ for VPS), and $d\omega$ is the area element [30]. Owing to the additive decomposition, we can interpret the last term in (1) as the stimulus-induced curvature potential $\mathcal{P}_\kappa = -2(1+\nu)h^2/3 \int \kappa \operatorname{tr}(\mathbf{b} - \mathring{\mathbf{b}})d\omega$. The surprisingly simple additive effect of natural curvature allows for a relatively straightforward extension of thin shells simulation methods to minimize (1) for a given stimulus κ. Indeed, by numerically minimizing Eq. (1), we find good quantitative agreement with the experimental shapes and the stimulus-induced transitions [Figs. 1(c) and 1(d)]. This suggests that the reduced-order model (1) is adequate to describe thin shells with curvature stimuli.

To theoretically understand how natural curvature interacts with the geometry and triggers the observed instabilities, we analyze the curvature potential and provide its geometrical interpretation. We start by expanding $\operatorname{tr}(\mathbf{b} - \mathring{\mathbf{b}})$ in terms of the displacement field $\boldsymbol{\Psi}$ up to first order [20]. Assuming a homogeneous natural curvature stimulus κ, the curvature potential decouples into bulk and boundary terms, $\mathcal{P}_\kappa = -\mathcal{W}_{\text{bulk}} - \mathcal{W}_{\text{edge}}$ [24]. For a sphere with outward pointing normal, they read

$$\mathcal{W}_{\text{bulk}} = -\frac{4(1+\nu)}{3}\left(\frac{h}{R}\right)^2\kappa\int \Psi_3 d\omega, \quad (2a)$$

$$\mathcal{W}_{\text{edge}} = \frac{2(1+\nu)}{3}h^2\kappa\oint\left(\mathbf{q} - \frac{\check{\boldsymbol{\Psi}}}{R}\right)\cdot\mathbf{t}\,ds, \quad (2b)$$

where Ψ_3 is the normal displacement, $\check{\boldsymbol{\Psi}}$ is the in-plane displacement field, and $\mathbf{t}$ is the outward normal vector to the boundary curve. The expression $\mathbf{q} = \nabla\Psi_3 - \check{\boldsymbol{\Psi}}/R$ represents the rotation of an element of the shell [20], such that $\mathbf{q} \cdot \mathbf{t}$ is the rotation of $\mathbf{t}$ [Fig. 1(b)]. The integral in (2a) is equivalent to the first-order energy of a pressure load. In the bulk, a curvature stimulus is therefore equivalent to an effective applied pressure. In (2a), κ is the work conjugate of the rotation $\mathbf{q} \cdot \mathbf{t}$ and the membrane in-plane displacement $\check{\boldsymbol{\Psi}} \cdot \mathbf{t}$, implying both a torquelike and membrane forcelike behavior. Specifically, for $\kappa > 0$, Eq. (2a) describes an outward torque at the boundary [Fig. 1(b)]. A similar interpretation holds for arbitrary open shells [24].

Numerically, we find that $|\mathcal{W}_{\text{edge}}| \gg |\mathcal{W}_{\text{bulk}}|$ for thin shells of all considered opening angles θ. We can rationalize this by considering small displacements. The Koiter

elastic energy then scales as $\bar{\mathcal{U}}^K \sim (\Psi_3/R)^2 R^2$, while the curvature potential scales as $\mathcal{P}_\kappa \sim h^2 \kappa (\Psi_3/R^2) R^2$ in the bulk. A balance of the two leads to $\Psi_3 \sim h^2 \kappa$. As the area of the shell is proportional to $R^2(1 - \cos\theta)$, the bulk work (2a) scales as $\mathcal{W}_{\text{bulk}} \sim h^4 \kappa^2 (1 - \cos\theta)$. Then, as the boundary layer is bending dominated [31], we obtain $|\mathbf{q} - \check{\Psi}/R| \sim \kappa\sqrt{Rh}$ [24], where $\sqrt{Rh}$ is the characteristic width of the boundary layer [20]. As the perimeter of the boundary is proportional to $R \sin\theta$, we conclude that the edge work (2a) scales as $\mathcal{W}_{\text{edge}} \sim h^4 \kappa^2 (R/h)^{3/2} \sin\theta$. By a comparison of the two scalings, we find $|\mathcal{W}_{\text{edge}}/\mathcal{W}_{\text{bulk}}| \sim (R/h)^{3/2}/\tan(\theta/2) \gg 1$; i.e., the boundary work dominates for the opening angles θ considered. Therefore, the boundary term dictates the observed shape transitions.

In experiments, we observe that snapping is indeed accompanied by minimal bulk deformation, but large rotation of the boundary. Moreover, we find that snap-through instabilities occur for open shells with $\theta \lesssim \pi/2$ when their tangent plane on the boundary becomes approximately horizontal (see the videos in the Supplemental Material [24]). In this state, the critical curvature within the boundary layer scales as $b_c \sim (1 + \nu)(-1/R + \kappa)$ [24]. Since the width of the boundary layer scales as $\sqrt{Rh}$, b_c must also scale as $\sim\theta/\sqrt{Rh}$. Thus we find the critical curvature stimulus at snapping $\kappa_s R \sim \bar{\theta}$, that is

$$\kappa_s R = \beta\bar{\theta} - \alpha, \tag{3}$$

leaving two scaling coefficients α and β to be determined later. For $\bar{\theta} \to 0$, shells tend to plates. Flat plates of radius r under curvature stimuli bifurcate at $\tilde{\kappa}_p h = \pm a(h/r)^2$ with $a = \sqrt{10 + 7\sqrt{2}}$ [17]. Then, for large R and small θ, but $r = R\theta$ finite, shells are expected to behave like plates if we identify $\tilde{\kappa}_p R = \kappa_p R - 1$; i.e., we compensate for the initial curvature $-1/R$. Therefore, shells will bifurcate at $\kappa_p R = \pm a/\bar{\theta}^2 + 1$, and we expect a symmetric bifurcation behavior around $\kappa R = 1$. Without loss of generality, we consider the case $\kappa < 0$, corresponding to the buckling of shells into spindlelike shapes. We define the critical curvature stimulus by κ_b, and now consider the behavior of deep shells. We note that for $\theta \to \pi$, the natural curvature will expend a torquelike work on a boundary whose perimeter approaches zero as $\sin\theta$, while the area of the shell to be deformed increases as $(1 - \cos\theta)$. The critical natural curvature will then diverge as $\kappa_b R \sim \tan(\theta/2) \sim 1/(\theta - \pi)$, that is, $1/(\bar{\theta} - \pi\sqrt{R/h})$. We conjecture that the curvature buckling of shells can be determined by combining the two diverging regimes for small and large $\bar{\theta}$ as

$$\kappa_b R = -\frac{a}{\bar{\theta}^2} + 1 + \frac{b}{\bar{\theta} - \pi\sqrt{R/h}} + c, \tag{4}$$

where a was given above, and b and c have to be determined by fitting to simulations. Notice that the superposition of

the two scalings retains the correct asymptotic behaviors as $\bar{\theta} \to 0$ and $\bar{\theta} \to \pi\sqrt{R/h}$.

Our theoretical scaling predictions can be summarized in a phase diagram (solid lines in Fig. 2) in the parameters $(\bar{\theta}, \kappa R)$, which fully characterize the curvature-induced instabilities of open shells. For $\kappa < 0$, the scaling law (4) with $b = 3.6$ and $c = -0.98$ provides the best fit with numerics, and agrees well with experiments. We note that a parameter-free determination of the buckling threshold would require a linear stability analysis, which is hampered due to the nontrivial fundamental state before buckling. For $\kappa > 0$, the behavior is richer: there are two phases of inverted curvature, one with broken rotational symmetry (blue region) and another phase that is rotationally symmetric (green). Simulations confirm the snapping transition (3) with $\alpha = 0.67$ and $\beta = 0.85$, but only if $\bar{\theta} > \bar{\theta}_s = 2.09$, in agreement with experiments. For $\bar{\theta} < \bar{\theta}_s$, we find that shells smoothly invert their curvature into the green phase as κ increases. This can be understood by considering a family of shells with a fixed h/R, and different θ. Since the width of the boundary layer scales as $\sqrt{Rh}$, shallower shells possess a boundary layer that covers a larger portion of the area compared to deeper shells. Thus, there exists a critical value $\bar{\theta}_s$ below which the boundary layer transitions into a wide region that covers the entire shell. As regions within the boundary layer are bending-dominated, the curvature of the shell smoothly follows the evolution of the spontaneous curvature for $\bar{\theta} < \bar{\theta}_s$. Starting from the green phase, rotational symmetry is eventually lost for large κR. The
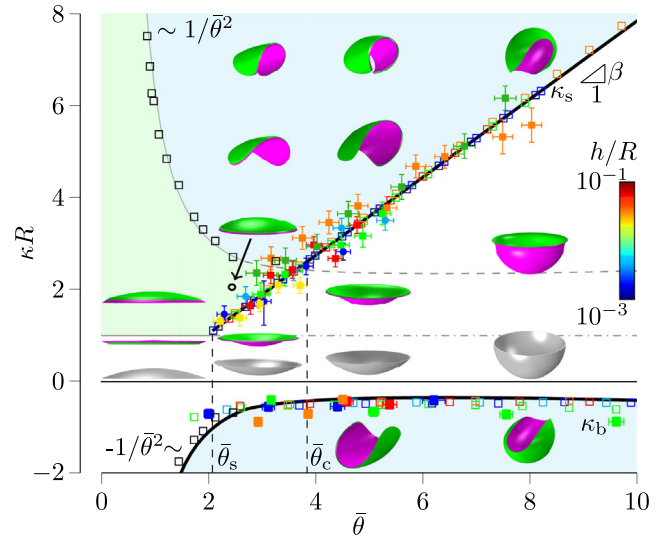

FIG. 2. Phase diagram of curvature-induced instabilities in open shells: white and green regions denote phases with rotational symmetry but opposite surface orientations, whereas blue regions denote phases of broken rotational symmetry. Theoretical transitions curves (solid lines) match well with experimental (colored full symbols) and numerical (colored empty symbols) findings, where color represents h/R.

transition line is well described by mirroring Eq. (4) around the axis of symmetry $\kappa R = 1$, as expected from the plate limit (dashed gray line), without any changes of the parameters b and c. At $\bar{\theta}_c$, this transition line intersects with Eq. (3), and a triple point emerges. Explicitly, the triple point is determined from $-\kappa_s + 2/R = \kappa_b$, which gives $\bar{\theta}_c = 3.85$, in agreement with experiments ($\bar{\theta}_c = 3.95 \pm 0.26$). Consequently, shells snap into a rotationally symmetric phase only if $\bar{\theta}_s < \bar{\theta} < \bar{\theta}_c$, whereas for $\bar{\theta} > \bar{\theta}_c$ shells immediately snap into an everted state of broken rotational symmetry (blue region). (Thin shells are unlikely to snap into cylindrical shapes [32]. However, we would expect the deformed shells have a small, nonzero curvature along one principal direction, corresponding to a near-isometric deformation with minimum energy.)

In contrast to open shells, only the bulk contribution remains for closed shells. Exploiting its analogy with pressure, we expect instabilities similar to the classical pressure-induced buckling of spherical shells [29,33–36]. More precisely, the bulk term is formally equivalent to the work done by an external (dead) pressure, $\mathcal{W}_p = -8(1-\nu^2)p/(Eh)\int \Psi_3 d\omega$ [2], allowing us to define an effective stimulus-induced pressure p via

$$\kappa h = 6(1-\nu)\left(\frac{R}{h}\right)^2 \frac{p}{E}, \qquad (5)$$

where E is the Young's modulus of the shell. Following this interpretation, a negative stimulus, $\kappa < 0$, corresponds to a negative external pressure, $p < 0$, thus causing an inflation of the shell. Conversely, a positive stimulus with $\kappa > 0$ is equivalent to positive external pressure and results in a compression of the sphere. By expanding the bending and stretching strains up to the first order in the displacement [20], and solving the Euler-Lagrange equations associated to (1), we find for the normal displacement $\Psi_3/h = -\kappa h/12 + O((h/R)^4)$ while the in-plane displacement is zero for symmetry. Having established the analogy to classical shell buckling [37,38], we expect a critical stimulus beyond which the shell will buckle in absence of any external load. It is tempting to identify the buckling natural curvature κ_b via (5) with the critical buckling pressure $p_b = 2E/\sqrt{3(1-\nu^2)}(h/R)^2$ obtained for the classical pressure buckling of spherical shells [37]. However, despite the formal analogy, pressure buckling and curvature buckling are triggered by fundamentally different residual stress states: while the residual stress in pressure-compressed shells is mainly of the membrane (in-plane) type, the prestress in curvature-compressed shells is a combination of membrane and bending stresses due to the evolving natural curvature that modifies the rest lengths of the body above and below the midsurface. A careful analysis then yields the critical buckling stimulus as

$$\kappa_b h = 4\sqrt{3\frac{1-\nu}{(1+\nu)(5+4\nu)}}, \qquad (6)$$

which for an incompressible material reduces to $\kappa_b h = 4/\sqrt{7}$ [24]. This is a large value, corresponding to a radius of natural curvature equal to two thirds of the thickness (via residual swelling we are experimentally limited to values of $|\kappa h| < 1/4$), yet it is comparable to natural curvatures observed during the eversion of the *Volvox* for which $\kappa h \simeq 2$ [21]. In contrast to open shells, where the characteristic curvature for snapping and buckling is $1/R$ due to the existence of nearly isometric deformations, the characteristic curvature in closed shells becomes $1/h$. To validate the buckling threshold, we performed simulations to minimize Eq. (1) using closed spheres for different values of thicknesses and radii such that $h/R \in [0.001, 0.1]$. Measuring Ψ_3/h as we vary κ, we confirm the behavior of $\Psi_3/h = -\kappa h/12$ before buckling [39], as well as the predicted critical curvature $\kappa_b h$ in Eq. (6) (Fig. 3). We note that, after buckling, the shell becomes unstable as the bifurcation is subcritical. To track the lowest-energy unstable branch in Fig. 3, we therefore minimized Eq. (1) using arc-length continuation while enforcing rotational symmetry (solid blue and red lines in Fig. 3). The postbuckling regime does not vary considerably with h/R and is similar to that observed in the pressure buckling of shells (insets in Fig. 3) [40].

In summary, we presented a theoretical and experimental study of curvature-induced instabilities in open and closed shells. Our theoretical analysis reveals that natural curvature can be interpreted as a combination of pressure and torque, and enables analytical predictions for instabilities in open and closed shells. We note that the critical stimuli in
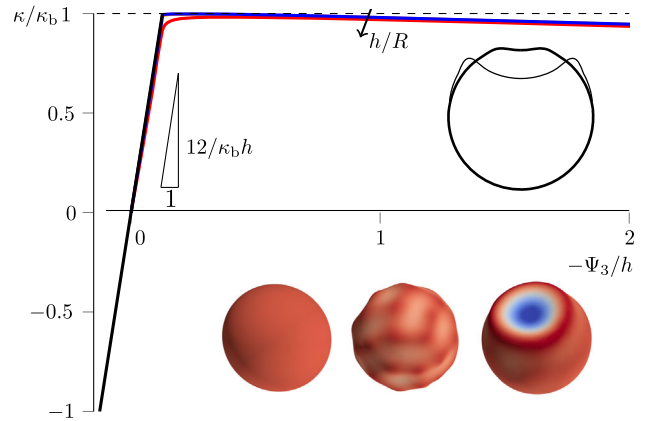
FIG. 3. Curvature buckling of a closed shell. As the stimulus κ/κ_b increases, the normal displacement at the north pole Ψ_3/h decreases linearly as predicted by theory. At $\kappa = \kappa_b$, buckling occurs and the shell becomes unstable. The solid black line represents theory, while the solid blue and red lines represent simulations for $h/R = 0.001, 0.1$, respectively. Axisymmetric profiles and 3D shapes from simulations are shown in the insets.

open and closed shells could also be determined via the method for nonlinear deformations presented in [13], and a formal comparison should be investigated in future work. We believe our study is a valuable contribution towards the generic understanding of curvature-driven instabilities in thin curved shells, as it generalizes previous experiments on plates [17] and elastica with a natural curvature [41]. Because of current limitations of the coating setup [18], we hope that our study will motivate experiments on more general surfaces, e.g., via the application of advanced 3D printing techniques [42]. For simple geometries, the presented experimental setup is extensible to nonhomogenous stimuli by local patterning of the individual layers. We hypothesize that, in the bulk, such stimuli remain at lowest order equivalent to normal forces, simplifying future theoretical analysis considerably. Lastly, the demonstrated precise control of shapes by means of natural curvature stimuli is scale invariant, and thus presents novel means towards the design of self-folding and deployable structures as well as instability-driven actuators in soft robotics applications across different length scales.

---

[*]dpholmes@bu.edu

[1] D. Bushnell and W. D. Bushnell, http://shellbuckling.com, 2017.

[2] W. T. Koiter, Proc. K. Ned. Akad. Wet., Ser. B: Phys. Sci. **72**, 40 (1969).

[3] E. Katifori, S. Alben, E. Cerda, D. R. Nelson, and J. Dumais, Proc. Natl. Acad. Sci. U.S.A. **107**, 7635 (2010).

[4] G. Lim H W, M. Wortis, and R. Mukhopadhyay, Proc. Natl. Acad. Sci. U.S.A. **99**, 16766 (2002).

[5] H. Liang and L. Mahadevan, Proc. Natl. Acad. Sci. U.S.A. **108**, 5516 (2011).

[6] T. Tallinen, J. Y. Chung, J. S. Biggins, and L. Mahadevan, Proc. Natl. Acad. Sci. U.S.A. **111**, 12667 (2014).

[7] A. Goriely, *The Mathematics and Mechanics of Biological Growth*, Interdisciplinary Applied Mathematics Vol. 45 (Springer, New York, 2017).

[8] N. C. Heer, P. W. Miller, S. Chanet, N. Stoop, J. Dunkel, and A. C. Martin, Development (Cambridge, U.K.) **144**, 1876 (2017).

[9] Y. Forterre, J. M. Skotheim, J. Dumais, and L. Mahadevan, Nature (London) **433**, 421 (2005).

[10] D. P. Holmes and A. J. Crosby, Adv. Mater. **19**, 3589 (2007).

[11] H. Yuk, S. Lin, C. Ma, M. Takaffoli, N. X. Fang, and X. Zhao, Nat. Commun. **8**, 14230 (2017).

[12] M. E. Gurtin, E. Fried, and L. Anand, *The Mechanics and Thermodynamics of Continua* (Cambridge University Press, Cambridge, England, 2010).

[13] M. B. Amar and A. Goriely, J. Mech. Phys. Solids **53**, 2284 (2005).

[14] A. Goriely and M. Ben Amar, Phys. Rev. Lett. **94**, 198103 (2005).

[15] E. Efrati, E. Sharon, and R. Kupferman, J. Mech. Phys. Solids **57**, 762 (2009).

[16] S. Armon, E. Efrati, R. Kupferman, and E. Sharon, Science **333**, 1726 (2011).

[17] M. Pezzulla, G. P. Smith, P. Nardinocchi, and D. P. Holmes, Soft Matter **12**, 4435 (2016).

[18] A. Lee, P. T. Brun, J. Marthelot, G. Balestra, F. Gallaire, and P. M. Reis, Nat. Commun. **7**, 11155 (2016).

[19] M. Pezzulla, S. A. Shillig, P. Nardinocchi, and D. P. Holmes, Soft Matter **11**, 5812 (2015).

[20] F. Niordson, *Shell Theory*, North-Holland Series in Applied Mathematics and Mechanics Vol. 29 (Elsevier Science, New York, 1985).

[21] S. Höhn, A. R. Honerkamp-Smith, P. A. Haas, P. K. Trong, and R. E. Goldstein, Phys. Rev. Lett. **114**, 178101 (2015).

[22] B. O'Neill, *Elementary Differential Geometry* (Academic Press, New York, 1997).

[23] M. Pezzulla, N. Stoop, X. Jiang, and D. P. Holmes, Proc. R. Soc. A **473**, 20170087 (2017).

[24] See Supplemental Material at http://link.aps.org/supplemental/10.1103/PhysRevLett.120.048002 for a detailed derivation, which includes Refs. [25–28].

[25] M. Deserno, Notes on Differential Geometry, https://www.cmu.edu/biolphys/deserno/pdf/diff_geom.pdf (2004).

[26] F. Cirak and M. Ortiz, Int. J. Numer. Methods Eng. **51**, 813 (2001).

[27] A. van der Neut, PhD thesis, Delft University of Technology, H.J. Paris, Amsterdam, 1932.

[28] A. van der Heijden, *W. T. Koiter's Elastic Stability of Solids and Structures* (Cambridge University Press, Cambridge, England, 2008).

[29] W. T. Koiter and J. G. Simmonds, in *Theoretical and Applied Mechanics: Proceedings of the 13th International Congress of Theoretical and Applied Mechanics, Moskow University, 1972*, edited by E. Becker and G. K. Mikhailov (Springer, Berlin, Heidelberg, 1973), pp. 150–176.

[30] J. Hanna, Bull. Am. Phys. Soc. **62** (2017).

[31] E. Efrati, E. Sharon, and R. Kupferman, Phys. Rev. E **80**, 016602 (2009).

[32] A. M. Abdullah, P. V. Braun, and K. J. Hsia, Soft Matter **12**, 6184 (2016).

[33] T. von Kármán and H. S. Tsien, J Aeronaut Sci **7**, 43 (1939).

[34] H. S. Tsien, J Aeronaut Sci **9**, 373 (1942).

[35] J. Thompson, Proc. K. Ned. Akad. Wet., Ser. B: Phys. Sci. **67**, 295 (1964).

[36] J. W. Hutchinson, J. Appl. Mech. **34**, 49 (1967).

[37] R. Zoelly, Ph.D. thesis, ETH Zürich, 1915.

[38] W. T. Koiter, Ph.D. thesis, Delft University of Technology, 1945.

[39] It is an open question to test whether a neo-Hookean material will be affected by limit point inflation instabilities triggered by $\kappa < 0$.

[40] J. W. Hutchinson, Proc. R. Soc. A **472**, 20160577 (2016).

[41] B. Audoly and Y. Pomeau, *Elasticity and Geometry: From Hair Curls to the Non-linear Response of Shells* (Oxford University Press, New York, 2010).

[42] Y. Mao, Z. Ding, C. Yuan, S. Ai, M. Isakov, J. Wu, T. Wang, M. L. Dunn, and H. J. Qi, Sci. Rep. **6**, 24761 (2016).